Monthly Notices
of the
ROYAL ASTRONOMICAL SOCIETY

MNRAS **493,** 1725–1735 (2020)
Advance Access publication 2020 February 14

doi:10.1093/mnras/staa344

Overconstrained gravitational lens models and the Hubble constant

C. S. Kochanek [1,2]★

[1]*Department of Astronomy, The Ohio State University, 140 West 18th Avenue, Columbus, OH 43210, USA*
[2]*Center for Cosmology and AstroParticle Physics, The Ohio State University, 191 W. Woodruff Avenue, Columbus, OH 43210, USA*

Accepted 2020 January 24. Received 2020 January 19; in original form 2019 November 12

ABSTRACT

It is well known that measurements of H_0 from gravitational lens time delays scale as $H_0 \propto 1 - \kappa_E$, where κ_E is the mean convergence at the Einstein radius R_E but that all available lens data other than the delays provide no direct constraints on κ_E. The properties of the radial mass distribution constrained by lens data are R_E and the dimensionless quantity $\xi = R_E\alpha''(R_E)/(1 - \kappa_E)$, where $\alpha''(R_E)$ is the second derivative of the deflection profile at R_E. Lens models with too few degrees of freedom, like power-law models with densities $\rho \propto r^{-n}$, have a one-to-one correspondence between ξ and κ_E (for a power-law model, $\xi = 2(n-2)$ and $\kappa_E = (3-n)/2 = (2-\xi)/4$). This means that highly constrained lens models with few parameters quickly lead to very precise but inaccurate estimates of κ_E and hence H_0. Based on experiments with a broad range of plausible dark matter halo models, it is unlikely that any current estimates of H_0 from gravitational lens time delays are more accurate than ∼10 per cent, regardless of the reported precision.

Key words: gravitational lensing: strong – cosmological parameters – distance scale.

1 INTRODUCTION

Refsdal (1964) pointed out that the time delays between multiple images in a gravitational lens could be used to determine the Hubble constant. There was a long delay before the discovery of the first lensed quasar (Walsh, Carswell & Weymann 1979) and then considerable controversy over the measurement of the first time delay (Schild 1990 versus Press, Rybicki & Hewitt 1992, resolved in favour of the former by Kundić et al. 1997). The measurement of delays is now routine (e.g. Bonvin et al. 2017, 2019; Courbin et al. 2018, recently) and the estimates are generally robust (e.g. Liao et al. 2015). The challenge lies in their cosmological interpretation. Individual lenses yield estimates of H_0 with reported precisions of 4–10 per cent (see Table 1) with higher precisions depending on averaging the estimates from large numbers of lenses. The present state of the art comes from the H0LiCOW Collaboration, who report a 2.4 per cent measurement of H_0 using six gravitational lenses (Wong et al. 2019).

The time delay Δt in a lens is roughly proportional to $H_0^{-1}(1-\kappa_E)$, where κ_E is the mean convergence (dimensionless surface density)[1] at the Einstein radius R_E (Kochanek 2002). Unfortunately, no gravitational lens observable other than the time delay directly constrains κ_E (see e.g. Gorenstein, Falco & Shapiro 1988; Kochanek 2002, 2006; Schneider & Sluse 2013; Sonnenfeld 2018; Wertz, Orthen & Schneider 2018), so some additional constraint on the mass distribution is required to determine H_0 from a time delay. It was quickly realized that stellar dynamical measurements, usually just meaning the central velocity dispersion, could provide this constraint (e.g. Grogin & Narayan 1996; Romanowsky & Kochanek 1999; Treu & Koopmans 2002).

If we explore simple lens models constrained by a stellar velocity dispersion σ_*, we find that the fractional uncertainty in H_0 is roughly equal to the fractional uncertainty in σ_*^2. Since the reported uncertainties in σ_* for the H0LiCOW lenses range from 6 to 10 per cent (see Table 1), H_0 should only be constrained to 12–20 per cent. The H_0 uncertainties reported by H0LiCOW of only 4–10 per cent (see Table 1) are, however, far smaller even after including all other sources of uncertainty in the models (e.g. time delays, the local environment, etc.). This means that the constraints on κ_E and thus H_0 must be coming from the lensing constraints on the mass model rather than the stellar dynamical constraints. In fact, the uncertainties in H_0 are so small compared to those in σ_*, that the stellar dynamical measurements must be making almost no contribution to the overall estimate of H_0.

As already noted, lensing data cannot determine κ_E – it is a fundamental degeneracy in the physics of gravitational lensing. Lens models determine κ_E only because the mathematical structure of any density model implies a relationship between the aspects of the model constrained by lens data and the surface density at the Einstein ring. If the density model has too few degrees of freedom compared to the number of lensing constraints, then one quickly obtains a very precise, but likely inaccurate, constraint on κ_E and H_0. Since the errors are systematic rather than random, there is also no reason to believe that they are reduced by averaging over multiple systems.

★ E-mail: ckochanek@astronomy.ohio-state.edu

[1]To be more precise, it is proportional to $1 - \langle\kappa\rangle$, where $\langle\kappa\rangle$ is the mean surface density in the annulus bounded by the lensed images.

Table 1. H0LiCOW lenses.

Lens	σ_* (km s^{-1})	H_0 (km s^{-1} Mpc^{-1})	References
HE 0435−1223	222 ± 15 (7%)	73 ± 6 (8%)	Wong et al. (2017)
PG 1115+080	281 ± 25 (9%)	83 ± 8 (10%)	Tonry (1998), Chen et al. (2019)
RX J1131−1231	323 ± 20 (6%)	80 ± 6 (8%)	Suyu et al. (2013)
SDSS 1206+4332	290 ± 30 (10%)	69 ± 4 (6%)	Agnello et al. (2016), Birrer et al. (2019)
B1608+656	260 ± 15 (6%)	71 ± 3 (4%)	Suyu et al. (2010)
WFI 2033−4723	250 ± 19 (8%)	72 ± 4 (6%)	Rusu et al. (2019)

Most of these points have been made previously (e.g. Kochanek 2006; Schneider & Sluse 2013; Xu et al. 2016; Unruh, Schneider & Sluse 2017; Sonnenfeld 2018). Here we make these arguments using a different set of analytic results and numerical experiments, which clearly show that the simple density models presently used for most inferences about H_0 from gravitational lens time delays suffer from these problems and become increasingly unreliable as the reported precision becomes smaller than ∼10 per cent. The arguments are presented in Section 2, and we summarize the results in Section 3.

2 THE ROLE OF PARAMETERS IN THE MASS MODEL

H0LiCOW basically uses two mass models for the lenses. The first model is a simple power law producing a deflection angle of $\alpha(\theta) = b^{n-1}\theta^{2-n}$. The model has two parameters, the Einstein radius b and the power-law index n, where $n = 2$ is the singular isothermal sphere (SIS) model. The second model combines the photometric model of the lens galaxy with a Navarro–Frenk–White (NFW; Navarro, Frenk & White 1997) profile

$$\rho \propto \frac{1}{r(a+r)^2} \tag{1}$$

for the dark matter halo. In theory, this model has three parameters, a mass-to-light ratio for the stellar profile, a density normalization for the NFW profile, and its scale length a. In practice, the scale length is constrained by a fairly strong prior to vary by only 10–15 per cent, which effectively makes this a two-parameter model as well.

In this section, we first review the basic problem that lensing data mathematically cannot determine the surface density κ_E needed to determine H_0 and derive the property of lens models that lens data do constrain. Next we illustrate the problem with a specific example of how mass models with small numbers of parameters can lead to increasingly precise but inaccurate estimates of κ_E. Finally, we show that a range of plausible models for dark matter haloes when modelled using the H0LiCOW mass distributions commonly have fractional systematic errors in H_0 of 10 per cent or more.

2.1 What do lens models measure?

We start by reviewing the basic problem. Consider a power-law model for circular lens with two images at r_1 and $-r_2$ ($r_1 \le r_2$). The lens equations require that

$$r_1 - b^{n-1}r_1^{2-n} = -r_2 + b^{n-1}r_2^{2-n}. \tag{2}$$

We can then solve for the Einstein radius,

$$b^{n-1} = \frac{r_1 + r_2}{r_1^{2-n} + r_2^{2-n}}. \tag{3}$$

Not surprisingly, with only one constraint, a solution can be found for any power-law index. If we have an additional set of images at r_3 and $-r_4$ ($r_4 \le r_3$ and $r_2 \le r_4 \le r_3 \le r_1$), then there is a unique solution from solving the transcendental equations

$$\frac{r_1 + r_2}{r_1^{2-n} + r_2^{2-n}} = \frac{r_3 + r_4}{r_3^{2-n} + r_4^{2-n}} \tag{4}$$

for the power-law index. Because the model has only two parameters, the mass distribution is now exactly defined everywhere up to the uncertainties in the position measurements. In particular, the convergence at the Einstein ring is now forced to be $\kappa_E = (3-n)/2$ that in turn forces a particular value for H_0 given a time delay. The mass distribution away from the Einstein ring is also fully specified, eliminating any important constraint from the dynamical data because the fractional uncertainties in lensing constraints are generally far smaller than the fractional uncertainties in velocity dispersions.

There are, however, two fundamental problems. First, as noted in the Introduction, whatever the available lensing constraints, the one quantity they do not directly constrain is the mean surface density needed to convert a time delay into H_0. The conversion of the lensing constraints into a value of κ_E is entirely set by the functional form of the mass model and its flexibility. Second, the lens geometry has absolutely no information on the mass distribution inside or outside the annulus encompassing the lens images – the exactly determined mass distribution for these regions is purely an extrapolation set by the functional form of the mass model.

These two points are also easily demonstrated non-parametrically (see Kochanek 2002, 2006). Let the mass of the lens between two radii be

$$m(r_1, r_2) = 2\int_{r_1}^{r_2} u\,du\kappa(u), \tag{5}$$

where $\kappa(r)$ is the convergence (surface density) profile of the lens. The deflection angle is then $\alpha(r) = r^{-1}m(0, r)$ and the lens equations require that

$$r_1 - r_1^{-1}m(0, r_1) = -r_2 + r_2^{-1}m(0, r_2). \tag{6}$$

Now $m(0, r_1) = m(0, r_2) + m(r_2, r_1)$, so

$$m(0, r_2) = r_1 r_2 - \langle\kappa\rangle_{21} r_2(r_1 - r_2), \tag{7}$$

where

$$\langle\kappa\rangle_{ij} = \frac{2}{r_j^2 - r_i^2}\int_{r_i}^{r_j} u\,du\kappa(u) \tag{8}$$

is the mean convergence in the annulus bounded by r_1 and r_2. For a thin annulus, the Einstein radius is $R_E^2 = r_1 r_2$ independent of the surface density, and the mean surface density is the quantity that determines the H_0 given the time delay since $H_0 \propto 1 - \langle\kappa\rangle_{21}$.

Stellar dynamics essentially provides an independent constraint on $m(0, r_2)$, thereby allowing an estimate of $\langle\kappa\rangle_{21}$ and hence H_0.

Adding additional lensing constraints does nothing to remove the degeneracy. Suppose r_1 and r_2 bound the region containing lensed images, and we again add an additional pair of lensed images with $r_2 < r_4 < r_3 < r_1$. There is now a second constraint equation like equation (6). The non-parametric parameters of the model are now $m(0, r_2)$, $\langle\kappa\rangle_{24}$, $\langle\kappa\rangle_{43}$, and $\langle\kappa\rangle_{31}$, leaving us with four parameters to be constrained by two equations. Viewed as a non-parametric model, the number of parameters expands faster than the number of constraints and the H_0 degeneracy problem cannot be eliminated no matter how many additional pairs of lensed images are added.

The annulus encompassing the lensed images of the quasar and its host is typically rather narrow, so using a simple functional form to describe the mass distribution in this annulus is likely quite reasonable. The problems are (1) that the constraints only apply over the annulus containing the lensed images – any prediction of the mass distribution beyond the annulus is purely an extrapolation, and (2) that they cannot constrain the quantity $\kappa_{\rm E}$ needed to determine H_0. We can illustrate this by first determining what property of a lens is constrained by the data, and then by constructing a model where two radically different radial mass distributions and predictions for H_0 are essentially indistinguishable using lens data.

Suppose we locally expand the deflection angle as a Taylor series near the Einstein radius, $R_{\rm E}$,

$$\alpha(r) \simeq R_{\rm E} + 2(\kappa_{\rm E} - 1)(r - R_{\rm E}) + \frac{1}{2}\alpha''_{\rm E}(r - R_{\rm E})^2, \tag{9}$$

where $\kappa_{\rm E}$ is the convergence and $\alpha''_{\rm E}$ is the second derivative of the deflection profile at $R_{\rm E}$. The lens equation for a source at radius β is then

$$\beta = -2(\kappa_{\rm E} - 1)(r - R_{\rm E}) + \frac{1}{2}\alpha''_{\rm E}(r - R_{\rm E})^2 \tag{10}$$

for one image and with the signs flipped on the right-hand side of the equation for the other image. We can divide both sides by $1 - \kappa_{\rm E}$, to get

$$\hat{\beta} = 2(r - R_{\rm E}) + \frac{1}{2}\hat{\alpha}''_{\rm E}(r - R_{\rm E})^2, \tag{11}$$

where $\hat{\beta} = \beta/(1 - \kappa_{\rm E})$ and $\hat{\alpha}''_{\rm E} = \alpha''_{\rm E}/(1 - \kappa_{\rm E})$. Since the source position β is not an observable, equation (11) means that for images near the Einstein ring, lens models determine $\hat{\alpha}''_{\rm E}$ and two lens models are indistinguishable if they have the same $\hat{\alpha}''_{\rm E}$. Alternatively, we can introduce the dimensionless quantity

$$\xi = R_{\rm E}\hat{\alpha}''_{\rm E} = \frac{R_{\rm E}\alpha''(R_{\rm E})}{1 - \kappa_{\rm E}} \tag{12}$$

as the second property of the radial mass distribution after $R_{\rm E}$ that can be well constrained by lens data. Because the uncertainties in $R_{\rm E}$ are generally small, the uncertainties in ξ will be dominated by the uncertainties in $\hat{\alpha}''_{\rm E}$.

Many previous studies have found that lens models modelled as a power law with $\rho \propto r^{-n}$ favour logarithmic slopes $n \simeq 2$ close to the $n = 2$ slope of an isothermal sphere (e.g. Rusin & Kochanek 2005; Gavazzi et al. 2007; Koopmans et al. 2009; Auger et al. 2010; Bolton et al. 2012). This does not mean that the typical slope of the density distribution on the scale of the Einstein radius has $n \simeq 2$. Instead, there is a one-to-one relation that $\xi = 2(n - 2)$ for the power-law models and the true physical constraint implied by finding $n \simeq 2$ is that $\xi \simeq 0$. It is again important to emphasize that lens models do not determine $\kappa_{\rm E}$, the quantity needed to estimate H_0. The functional form chosen for the mass model implies some value of $\kappa_{\rm E}$ given the value of ξ, but a different mass model will lead to a different value of $\kappa_{\rm E}$ for the same value of ξ. For the power-law models, $\kappa_{\rm E} = (3 - n)/2 = (2 - \xi)/4$, with $\kappa_{\rm E} = 1/2$ for $n = 2$ or $\xi = 0$. However, a different mass model will predict a different value of $\kappa_{\rm E}$ for the same value of ξ.

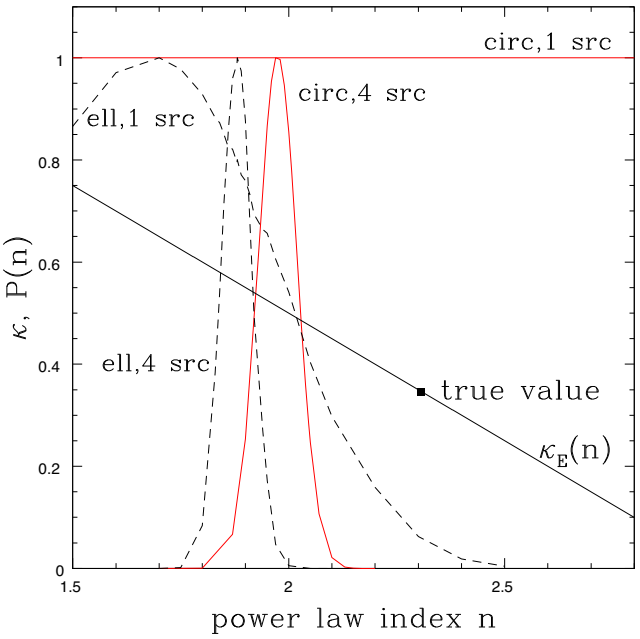

Figure 1. Probability of the power-law index n for a Hernquist (1990) model lens with an Einstein radius of $R_{\rm E} = 1.3s$ for circular (red, solid) and ellipsoidal (black, dashed) models fitting either one source producing two images ('1 src') or four sources producing 12 images ('4 src'). For the circular lens, matching the values of ξ predicts that the best-fitting power-law model should have $n = 2$. The solid line shows the dependence of the convergence at the Einstein radius $\kappa_{\rm E}(n)$ on the power-law index, where the point labelled 'true value' is the correct value for the input model.

2.2 A demonstration of the problem

Consider the Hernquist (1990) model,

$$\rho \propto \frac{1}{r(s + r)^3}, \tag{13}$$

where the scale radius is related to the effective radius by $s \simeq 0.55R_{\rm e}$. For a Hernquist (1990) model lens, the value of ξ depends on the position of the Einstein radius relative to the break radius $R_{\rm E}/s$, and $\xi = 0$ for $R_{\rm E}/s \simeq 1.3$, where $\kappa_{\rm E} \simeq 0.35$ is the convergence. If we model this lens as a power law, we should find that $n \simeq 2$ with $\kappa_{\rm E} \simeq 0.5$ as the convergence. This means that the power-law lens model will produce a fractional error in H_0 of $f = H_{\rm true}/H_{\rm model} - 1 \simeq 30$ per cent.

Fig. 1 shows a sequence of four cases fitting this example of a Hernquist (1990) lens model with a power-law model. We ignore the generation of faint third images by the Hernquist (1990) model and the flux ratios of the images. For computing a goodness of fit, we assume astrometric uncertainties of $0.003s$ for the image and lens positions and no constraints on the ellipticity of the lens or the external shear for the ellipsoidal models. The shear and ellipticity parameters remain reasonable without additional constraints. We fit the fake data using LENSMODEL (Keeton 2001, 2011) with the χ^2 goodness of fit computed on the image plane.

We first considered two circular lens models. In the first, we place one image at $1.1R_{\rm E}$, which has a second image at $-0.89998R_{\rm E}$. Note that the image separation of $1.9998R_{\rm E}$ is essentially indistinguishable from the $2R_{\rm E}$ that would be produced by an SIS model. As seen in Fig. 1, this data can be perfectly fit ($\chi^2 \equiv 0$) independent of the slope of the power law as expected from equation (3). For the second model, we added three additional sources that produced outer images at $1.05R_{\rm E}$, $1.2R_{\rm E}$, and $1.3R_{\rm E}$, respectively. The separations of the three resulting image pairs are also essentially indistinguishable from the $2R_{\rm E}$ prediction of an SIS model. If we fit these four image pairs, we now find that the model is strongly constrained to have $n = 2$, as expected from matching the values of ξ. The best model ($n = 1.974$) is still a perfect fit with $\chi^2 = 0.015$ for 3 degrees of freedom. The surface density at the Einstein ring implied by the model is, however, completely wrong, leading to a 30 per cent error in H_0. Adding more lensing constraints will never solve the problem – the χ^2 distribution will simply steadily narrow around $n \simeq 2$ with smaller and smaller uncertainties in both n and the implied value of $\kappa_{\rm E}$.

We next considered the same cases but with an ellipsoidal lens in an external shear. We gave the Hernquist (1990) model a surface density axial ratio of $q = 0.65$ and added an external shear of $\gamma = 0.05$ at a randomly chosen angle. For the ellipsoidal models, we view s as the intermediate axis scale length and again normalize the mass so that $R_{\rm E} = 1.3s$ (LENSMODEL uses the major axis scale length of $sq^{-1/2}$ to define the models). We again placed images at $1.05R_{\rm E}$, $1.1R_{\rm E}$, $1.2R_{\rm E}$, and $1.3R_{\rm E}$ and random angles around the lens and then found their companion images. The two images closer to $R_{\rm E}$ produced four images, and the two further from $R_{\rm E}$ produced two images, so we now have 12 images in total.

We first repeated the fits using the four-image system associated with an image at $1.1R_{\rm E}$. We again find a good fit, but at $n \simeq 1.7$ with $\chi^2 = 0.004$. Formally, the model has fewer constraints than parameters (-1 degrees of freedom). The goodness of fit is not independent of n but clearly selects a preferred range, albeit with relatively large uncertainties. We are confident that this is a consequence of the limited degrees of freedom in the angular structure of the mass model. The density distribution of the Hernquist (1990) model out to $R_{\rm E}$ drops more slowly than the $n = 2$ power-law model, so for the same quadrupole it will have larger higher order multipoles. The power-law models compensate by shifting to lower n, less centrally concentrated mass distributions. Kochanek (2006) has an extensive discussion on the angular structure of lens models.

If we now add in the other three sources and fit all 12 images, Fig. 1 shows that n is again tightly constrained but still offset to lower n than the circular models. The sense of the shift only exacerbates the problems for H_0, since these models have surface densities at $R_{\rm E}$ even higher than the $n = 2$ SIS model and so are still further from the input model. The best-fitting models at $n \simeq 1.88$ are statistically good fits with $\chi^2 = 3.3$ for 3 degrees of freedom. Adding additional sources producing multiple images simply narrows the probability distribution $P(n)$.

Fig. 2 shows the consequences of adding dynamical constraints to the lensing constraints illustrated in Fig. 1. We assume a measured dispersion equal to the true dispersion for a Hernquist (1990) model inside the aperture $R < s$ with a 10 per cent uncertainty. The circular model with only one two-image lens system plus dynamics comes closest to yielding models with the correct value of $\kappa_{\rm E}$, since the joint probability distribution is simply the dynamical probability distribution as the lens model imposes no constraint on n. For the elliptical model with one four-image lens system, the dynamical constraint shifts the lensing distribution to be more

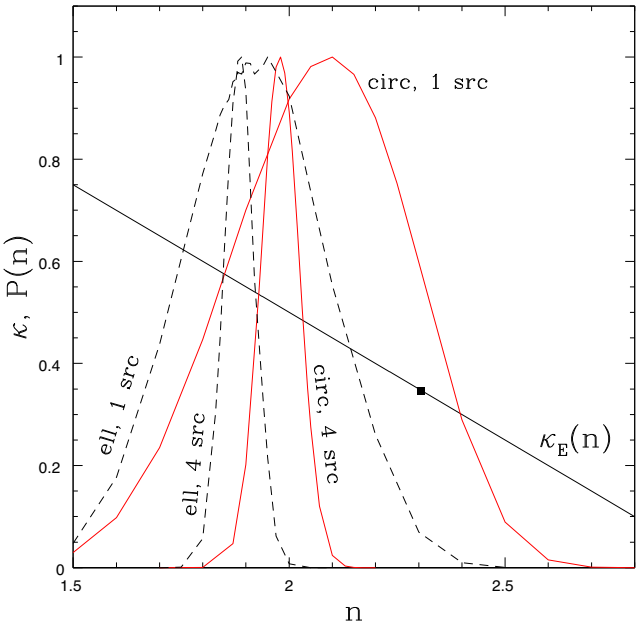

Figure 2. Changes in the probability distributions for n from Fig. 1 after adding a 10 per cent estimate of the velocity dispersion centred on the true value. The models are labelled as in Fig. 1. The dynamical constraints shift the probability distributions to better agree with the true value if the lens constraints are weak (only one source), but the changes are negligible when the lens constraints are strong (four sources). For the circular single-source model, the probability peaks at the value of n producing the input velocity dispersion.

consistent with the correct value of $\kappa_{\rm E}$. For both the circular and ellipsoidal models with four sources, the probability distributions are essentially unchanged after adding the dynamical constraint. The lens model is so strongly constrained by the lens data that the relatively weaker dynamical constraints have little effect.

We tried a broad range of additional numerical examples for a range of mass models. In circular models, the solution always converges to match the ξ of the input model. In ellipsoidal models with external shear, there are modest shifts from the ξ of the input model. These experiments explain the puzzle discussed in the Introduction. In mass models with few degrees of freedom and very strong lensing constraints, the lens data 'pins' the mass model to match the ξ required by the data. The weaker dynamical constraints then have little effect and estimates of H_0 (i.e. $\kappa_{\rm E}$) show little sensitivity to changes in the velocity dispersion. Unfortunately, Figs 1 and 2 also show that the accuracy of the estimate of H_0 was greatly reduced rather than enhanced by the use of the additional strong lensing constraints.

2.3 Consequences

By matching lens models in ξ, it is now easy to show the consequences of using different mass models in the case of circular lenses. We used an input mass distribution consisting of a de Vaucouleurs (1948) (deV) model for the stars plus a dark halo. Qualitatively similar results are obtained if we chose a different density distribution for the stars. We scaled everything by the effective radius $R_{\rm e}$ of the deV model and generated models with 0, 25, or 50 per cent of the mass inside the Einstein radius $R_{\rm E}$ coming from the halo. We considered four halo models. The first is simply the NFW model of equation (1). The second is the generalization

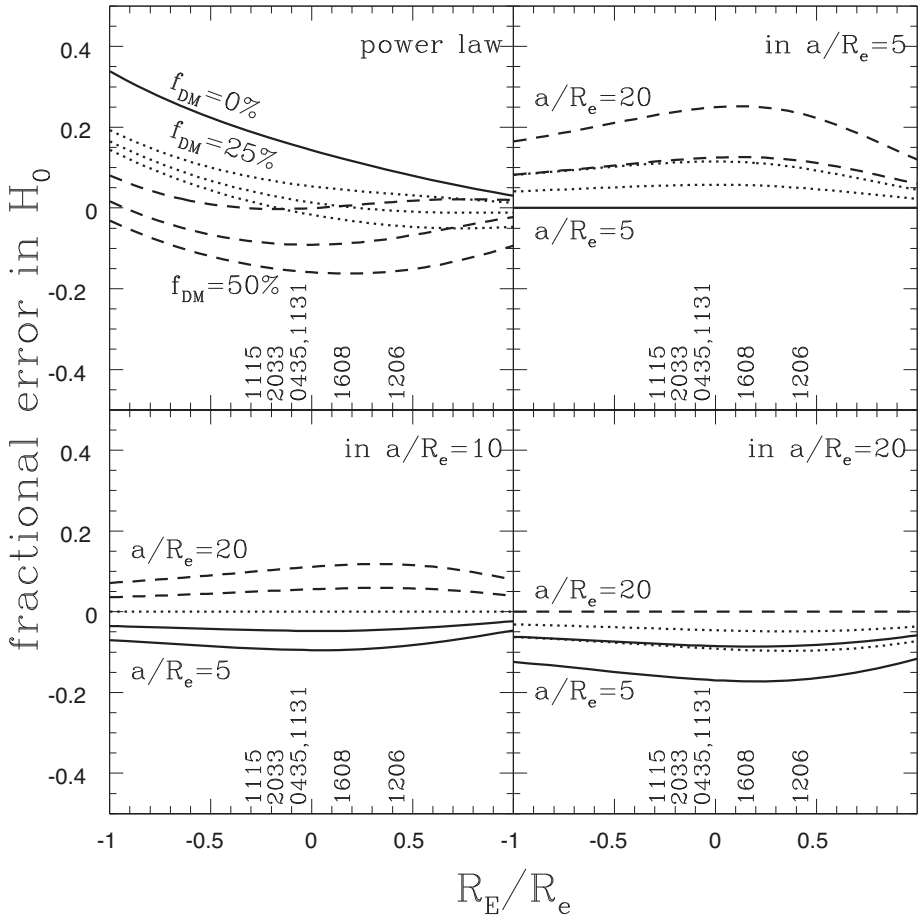

Figure 3. Fractional errors in H_0 for an input deV+NFW halo modelled as a power law (top left) or a deV+NFW halo model (other panels). In the power law panel the dark matter fraction is $f_{\rm DM} = 0$ per cent (solid), 25 per cent (dotted), or 50 per cent (dashed) for input NFW scale lengths of $a/R_{\rm E} = 5$ (top), 10 or 20 (bottom). For the NFW panels, the input NFW scale length is $a/R_{\rm E} = 5$ (top right) 10 (lower left), or 20 (lower right), and the model NFW scale length is $a/R_{\rm E} = 5$ (dotted), 10 (solid), or 20 (dashed) in each panel. Results are shown for dark matter fractions of $f_{\rm DM} = 25$ or 50 per cent with larger fractional errors for larger dark matter fractions. When $f_{\rm DM} = 0$ per cent or the input and model NFW scale lengths are the same, the fractional error is zero. The locations of the H0LiCOW lenses in $R_{\rm E}/R_{\rm e}$ are indicated by the lens names.

of the NFW (gNFW) profile

$$\rho \propto \frac{1}{r^{\gamma}\left(a^2 + r^2\right)^{(m-\gamma)/2}} \tag{14}$$

introduced as a lens model by Muñoz, Kochanek & Keeton (2001). This asymptotically matches generalizations of the NFW model at large and small radii, but the change in structure near the break radius makes the deflection profiles analytic. The case $\gamma = 1$, $m = 3$ is similar to the NFW model, while $\gamma = 3/2$, $m = 3$ is similar to the model favoured by Moore et al. (1999). The third is the Einasto (1965) profile

$$\rho \propto \exp\left[-\frac{2}{\alpha}\left(\left(\frac{r}{a}\right)^{\alpha} - 1\right)\right], \tag{15}$$

where $0.15 \lesssim \alpha \lesssim 0.30$ models may better fit halo simulations than the NFW model (e.g. Merritt et al. 2005; Navarro et al. 2010; Reed, Koushiappas & Gao 2011). The Einasto (1965) models are most easily treated numerically.

These first three models are for dark matter haloes unaffected by baryons, but the actual halo structures of galaxies are modified by the presence and evolution of the baryons. In particular, the baryons adiabatically compress the dark matter orbits as they cool and shrink relative to the dark matter. As a fourth halo model, we use the simple model of adiabatic compression from Blumenthal et al. (1986). We start with an NFW halo and make the final distribution of the baryons a Hernquist (1990) density profile with the same effective radius as the deV model we use for the lens model. We use a NFW concentration of $c = 10$, so that the virial radius is $r_{\rm v} = ca = 10a$, and a baryonic mass fraction of 15.7 per cent (Planck Collaboration VI 2018). We then combine this adiabatically compressed NFW profile with the deV model for the stars, again assuming that either 25 or 50 per cent of the projected mass inside the Einstein ring comes from the halo – we did not force the dark matter fraction implied by the adiabatically compressed model.

Following H0LiCOW, we model the input system using either the power-law mass distribution ('PL') or the input stellar distribution, here a de Vaucouleurs (1948) model, combined with an NFW model for the halo ('deV+NFW'). We assumed that the effective radii of the two deV models were fixed and identical. With the break radius a of the NFW model fixed, both mass models have two parameters that we determine by matching the Einstein radius and ξ of the input model as function of the Einstein radius relative to the effective radius $R_{\rm E}/R_{\rm e}$. Given the input $\kappa_{\rm input}$ and model $\kappa_{\rm model}$ surface densities at the Einstein radius, we can then compute the

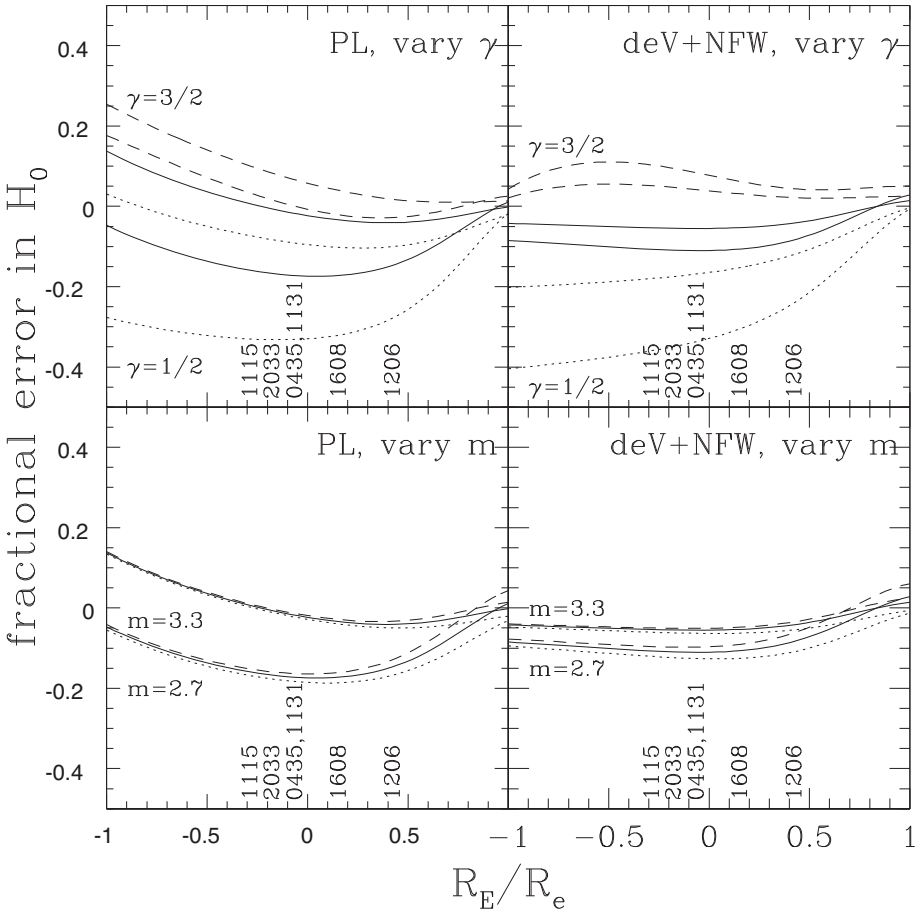

Figure 4. Fractional errors in H_0 for an input deV+gNFW halo modelled as a power law ('PL', left-hand panels) or a deV+NFW halo model (deV+NFW, right-hand panels). In the top panels, the asymptotic slope $m = 3$ is fixed and the inner density slope exponent of the gNFW model is $\gamma = 1/2$ (dotted), $\gamma = 1$ (solid), or $\gamma = 3/2$ (dashed). In the lower panels, the inner exponent is fixed to $\gamma = 1$ while the asymptotic slope is $m = 2.7$ (dotted), $m = 3$ (solid), and $m = 3.3$ (dashed). The scale length is fixed to $a/R_e = 10$ for both the gNFW and NFW models and the dark matter fraction is either $f_{DM} = 25$ or 50 per cent, with larger fractional errors for larger f_{DM}.

fractional error in H_0 as

$$f = \frac{H_{\rm true}}{H_{\rm model}} - 1 = \frac{1-\kappa_{\rm input}}{1-\kappa_{\rm model}} - 1. \quad (16)$$

This has the sense that the models underestimate (overestimate) H_0 if $f > 0$ ($f < 0$).

We first consider models where the input halo is NFW using input break radii of $a/R_E = 5$, 10, and 20. H0LiCOW sets $a \simeq (58 \pm 8)\ h^{-1}$ kpc based on the stacked weak lensing analysis of the Sloan Advanced Camera for Surveys (ACS) lens sample by Gavazzi et al. (2007). This roughly corresponds to $a/R_e \simeq 10$ for most of the H0LiCOW lenses. Whether from Gavazzi et al. (2007) or simulations (e.g. Bullock et al. 2001; Reed et al. 2011; Dutton & Macciò 2014), $a/R_e \simeq 10$ is roughly the correct scale. However, while the 15 per cent uncertainty in a found by Gavazzi et al. (2007) and used by H0LiCOW may be a realistic estimate of the uncertainty in the mean scale length, it greatly underestimates the plausible range of scale lengths for individual lenses. The lens galaxies have a finite spread in halo mass, and halo concentrations have significant scatter at fixed halo mass (e.g. Dutton & Macciò 2014). There are further dependencies on the redshifts of formation and observation. Hence, the factor of 2 range around $a/R_e = 10$ we use for illustration is relatively realistic even if $a/R_e = 10$ is the true mean halo scale length of lenses. Fig. 3 shows fractional errors from modelling these lenses using either a power-law model or deV+NFW models with the same three break radii.

If lenses happen to have deV+NFW mass distributions with $f_{DM} = 25$ per cent and $a/R_E = 10$, then the power-law models do remarkably well, with fractional errors of only 1–2 per cent for the range of R_E/R_e spanned by the lenses. However, for any other dark matter fraction or scale length, the fractional errors quickly exceed 5 per cent. The exact values of the systematic errors found for the power-law models are quite sensitive to changing the stellar mass distribution. For example, for this deV+NFW model, the fractional error for $R_E = 1.3s = 0.72R_e$ is 15 per cent instead of the 30 per cent fractional error we found for the same Einstein radius in the Hernquist (1990)+NFW model of Section 2.2.

The other three panels of Fig. 3 show the results for the deV+NFW model and the consequences of differences in the NFW break radius. If the input and model break radii match, or there is no dark matter ($f_{DM} = 0$ per cent), then the lens model can exactly reproduce the input model and the fractional errors are zero. However, if the lens model scale length is greater (less) than the true scale length, H_0 is underestimated (overestimated) with the magnitude of the error increasing with the dark matter fraction. Changing the stellar distribution, but still using the same stellar mass distribution to both generate and model the lens, seems to

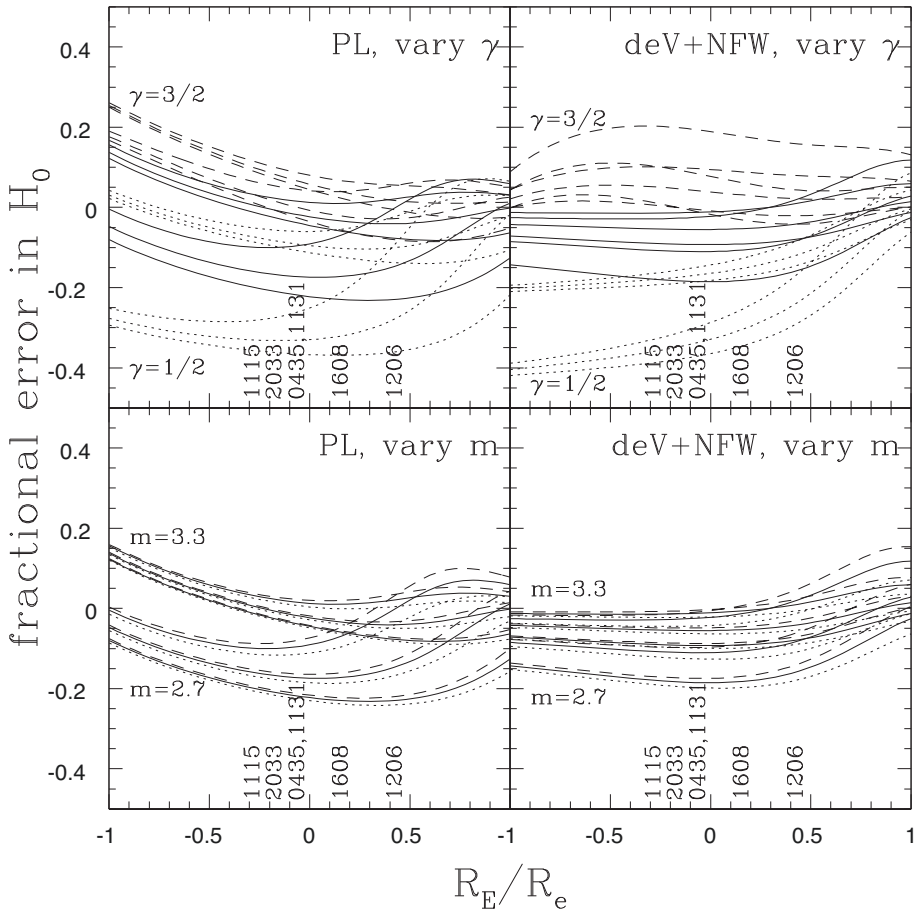

Figure 5. As in Fig. 4 but adding the results for both models having $a/R_e = 5$ and 20. The same halo scale length is still used for both input gNFW and model NFW profiles. The spread increases further if we allow the scale lengths to differ as in Fig. 3.

have little effect on systematic errors found when modelling the system by the stellar density plus an NFW halo.

Next we consider the gNFW models (equation 14), where we can vary the inner (γ) and outer (m) logarithmic slopes of the profile and the scale length a. Fig. 4 shows the results where both the gNFW and NFW profiles have $a/R_e = 10$. The first point to note is that even with the same scale length and exponents matching those of the NFW profile ($\gamma = 1, m = 3$), there are significant changes in the fractional errors for H_0 whether using the power-law or deV+NFW models. As before, the shifts increase as the dark matter fraction increases. Varying the outer slope m has relatively little effect on the results for the $2.7 \leq m \leq 3.3$ range shown. Varying the inner slope over the range $1/2 \leq \gamma \leq 3/2$ creates quite large shifts, where the models tend to underestimate (overestimate) H_0 as we make the inner profile steeper (shallower). The limit $\gamma = 3/2$ is the slope favoured by Moore et al. (1999). As shown in Fig. 5, changing the scale length a to $a/R_e = 5$ or $a/R_e = 20$ produces significant changes compared to $a/R_e = 10$ even though we continue to use the same break radius for both the input gNFW mass model and the lens NFW model. We do not show the cases where we allow the two break radii to differ, but this leads to still broader ranges for the fractional errors that are qualitatively similar to the effects for the deV+NFW models in Fig. 3.

Fig. 6 shows the results for the Einasto (1965) halo models with a dark matter fraction of $f_{DM} = 25$ per cent. The fractional errors depend on the parameter α, shifting towards more positive fractional errors as α is reduced. As with the other halo models, more compact haloes and haloes of one scale length modelled by one with a smaller scale length are also shifted towards more positive fractional errors. The typical scale of the systematic errors for $f_{DM} = 25$ per cent is again of order 10 per cent for reasonable ranges of the model parameters, rising to ∼20 per cent for $f_{DM} = 50$ per cent.

Fig. 7 shows the results for the adiabatically compressed NFW haloes with a dark matter fraction of $f_{DM} = 25$ per cent. The adiabatically compressed haloes are more centrally concentrated, so it is not surprising that the main qualitative change from the NFW models in Fig. 3 is to shift the fractional errors to larger positive values. The qualitative shifts seen in Fig. 7 are also found if we adiabatically compress the Einasto (1965) profiles and are presumably generic.

So far, we have assumed that the shape of the stellar density distribution is exactly the same in both generating and modelling the lens, leaving only the mass-to-light ratio as a parameter of the lens models. Photometric models of the lens galaxies generally leave small fractional residuals, so if the stellar distributions have constant mass-to-light ratios this is likely a safe assumption until pursuing ∼1 per cent fractional uncertainties in H_0. However, it is routine to find that surface brightness profiles depend on the filter of observation or equivalently that early-type galaxies have colour gradients indicative of radial changes in age or metallicity that in turn imply changes the stellar mass-to-light ratio (see e.g. the review by Kormendy & Djorgovski 1989) Thus, as a final experiment, we

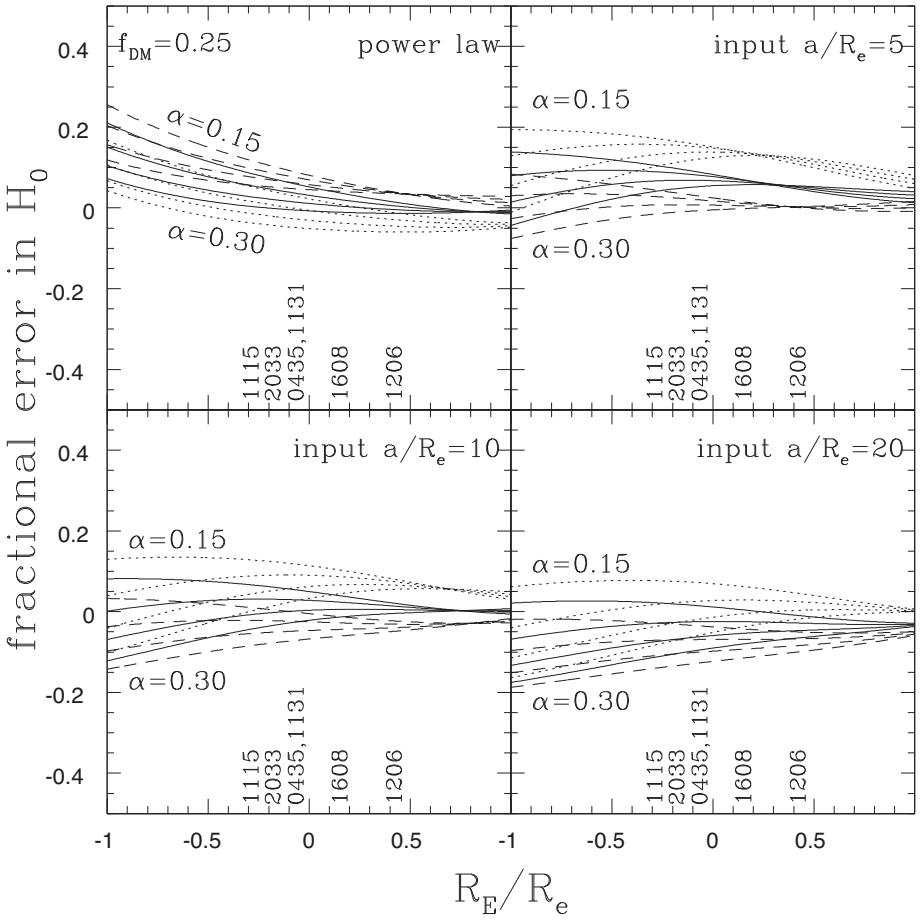

Figure 6. Fractional errors in H_0 for deV+Einasto models with $f_{DM} = 25$ per cent and $\alpha = 0.15$, 0.20, 0.25, and 0.30. The top left-hand panel uses power-law models for Einasto haloes with $a/R_e = 5$ (dashed), 10 (solid), and 20 (dotted). The remaining panels show deV+NFW models applied to Einasto profiles with $a/R_E = 5$ (top right), 10 (lower left), and 20 (lower right). The NFW models use $a/R_e = 5$ (dashed), 10 (solid), and 20 (dotted).

gave the input stellar mass distribution a gradient in its mass-to-light ratio. We multiplied the input deV density distribution by

$$1 + \mu \left(\frac{R - R_e}{R_e} \right) \tag{17}$$

but modelled the stellar mass distribution using just the input deV density distribution (i.e. $\mu \equiv 0$). For illustration we used $\mu = \pm 0.2$, so a 20 per cent change in the mass-to-light ratio per effective radius. We did not worry about the mass-to-light ratio becoming negative for large radii when $\mu < 0$, as all that matters is the mass-to-light ratio from the centre to R_E, and the Einstein radii are well inside the radius where the model becomes problematic. As shown in Fig. 8, modest gradients in the stellar mass-to-light ratio can easily lead to 5–10 per cent systematic errors in estimates of H_0 even if the photometric profile of the lens in some filter is exactly known.

3 DISCUSSION

Estimates of H_0 from lens time delays are controlled by the convergence (surface density) κ_E at the Einstein radius R_E, with $H_0 \propto 1 - \kappa_E$. No differential lens data (image separations, flux ratios, etc.) other than the time delays *ever* directly constrains κ_E – it is a fundamental degeneracy in the mathematics of lensing (see e.g. Gorenstein et al. 1988; Kochanek 2002, 2006; Schneider & Sluse 2013; Wertz et al. 2018). Lens data constrain two properties of the radial mass distribution: (1) the Einstein radius R_E; and (2) the dimensionless number $\xi = R_E \alpha''(R_E)/(1 - \kappa_E)$, where $\alpha''(R_E)$ is the second derivative of the deflection profile at the Einstein radius. Any lens with constraints from more than one set of lensed images will strongly constrain R_E and ξ. If the (radial) mass model has only two parameters, this will also lead to tight constraints on κ_E and hence H_0 because the model has no additional degrees of freedom. For example, in power-law lens models with deflection profiles $\alpha(R) = b^{n-1} R^{2-n}$, $R_E = b$, $\xi = 2(n - 2)$, and $\kappa_E = (3 - n)/2 = (2 - \xi)/4$. But the constraint on κ_E is purely dictated by the mathematical structure of the lens model and not by the lens data. We demonstrate this point in detail for a particular model, admittedly chosen to lead to an alarming 30 per cent fractional error in H_0.

We carried out an extensive survey of the consequences of using strong lens constraints by simply matching R_E and ξ between mass models. For the input models, we considered lenses consisting of a de Vaucouleurs (1948) model combined with a broad range of physically reasonable halo models [the Navarro et al. (1997) NFW model, generalizations of the NFW model, the Einasto (1965) model, and an adiabatically compressed NFW model]. We then determined the corresponding best fit that would be found using the two standard H0LiCOW lens models: the power-law model or the combination of the input de Vaucouleurs (1948) model with

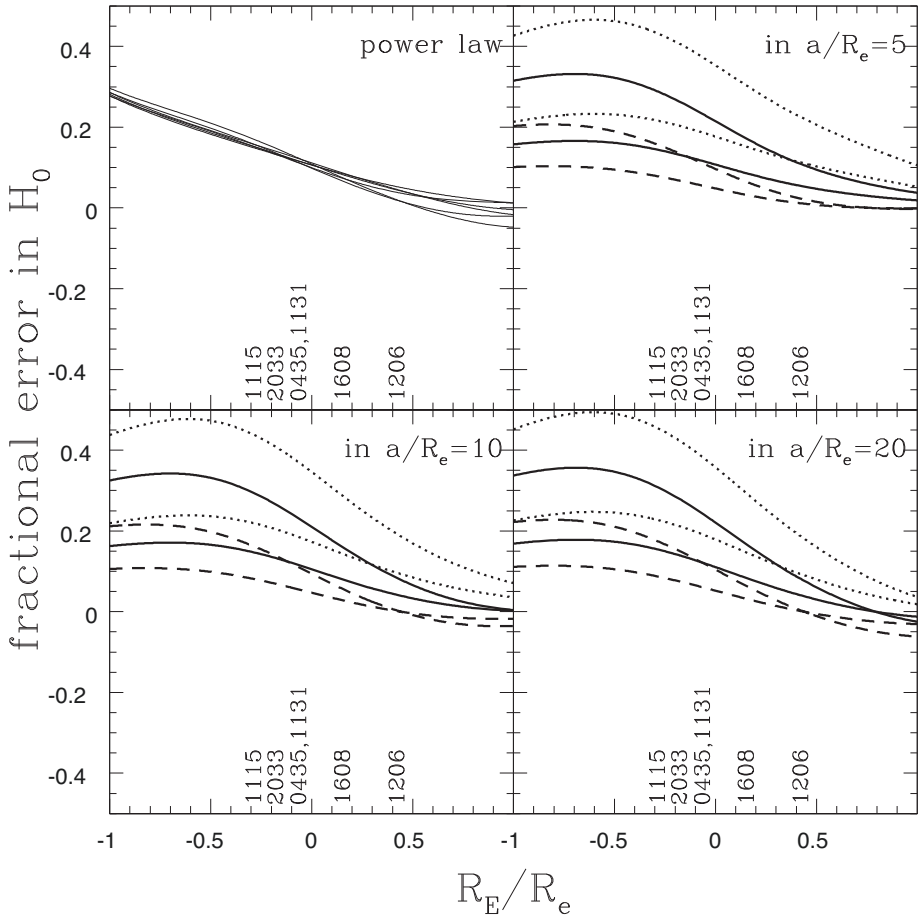

Figure 7. Fractional errors in H_0 for adiabatically compressed NFW haloes. The top left-hand panel shows the results for the power-law models and the other three panels are for the deV+NFW models where the input model has $a/R_{\rm E} = 5$ (top right), 10 (lower left), or 20 (lower right) and the lens model has $a/R_{\rm E} =$ 5 (dashed), 10 (solid), or 20 (dotted). All panels include both the $f_{\rm DM} = 25$ and 50 per cent cases.

an NFW halo. From the difference between the true and model values of $\kappa_{\rm E}$ we can estimate the resulting fractional error in H_0. The typical scale of the systematic error in H_0 is ∼10 per cent. On the one hand, this seems remarkably good given the simplicity of the mass models. On the other hand, it also means that the accuracy of all current estimates of H_0 from gravitational lens time delays is ∼10 per cent independent of the reported precision of the measurement.

As emphasized by Schneider & Sluse (2013), using mass models with additional degrees of freedom, so that determining $R_{\rm E}$ and ξ does not force a particular value of $\kappa_{\rm E}$ in our language, is the easiest way to ensure that the precision of the measurement does not exceed the accuracy even in the presence of very strong constraints from the lens data. The power-law model should clearly simply be abandoned – while it is adequate for ∼10 per cent estimates of H_0 it is essentially useless if higher accuracies are needed. Combining the stellar distribution with an NFW model can capture much of this uncertainty if the scale radius of the NFW component is allowed a significant dynamic range. The current H0LiCOW models generally constrain the scale length to 10–15 per cent, essentially making it a two-parameter model like the power-law models. Even to the extent that NFW models are correct, the scatter of lenses in mass and the spread of concentrations seen at fixed mass mean that the scale length should really be allowed to vary by a factor of ∼2.

While we have emphasized the radial structure of the density distribution because it then allows us to carry out a large model survey, one should have similar concerns about the number of degrees of freedom in the angular structure. In our example from Section 2.2 of a lens producing a large fractional error in H_0, the problems only worsened when we considered a non-circular version of the same lens. The angular structure of the lens drove the models to have a radial density distribution with $\kappa_{\rm E}$ even more divergent from the true value than in the circular models. Models need to have enough angular degrees of freedom that the angular structure beyond the quadrupole is not largely determined by the radial mass distribution of a single ellipsoidal density distribution (see Kochanek 2006).

There will remain a fundamental problem. While mass models with more degrees of freedom can capture the uncertainties in H_0 created by the uncertainties in halo structure, these are largely systematic rather than random problems. For example, if haloes were truly NFW models with a factor of 2 random scatter in the NFW scale length, then we might legitimately average the results from multiple lenses to produce a joint estimate of H_0 with smaller uncertainties than for the individual lenses. However, if the freedom from allowing a broad range of scale lengths is really compensating for the fact that the real mass distribution is systematically different from the mean behaviour of the model, then there is no reduction in the uncertainties from averaging multiple lenses.

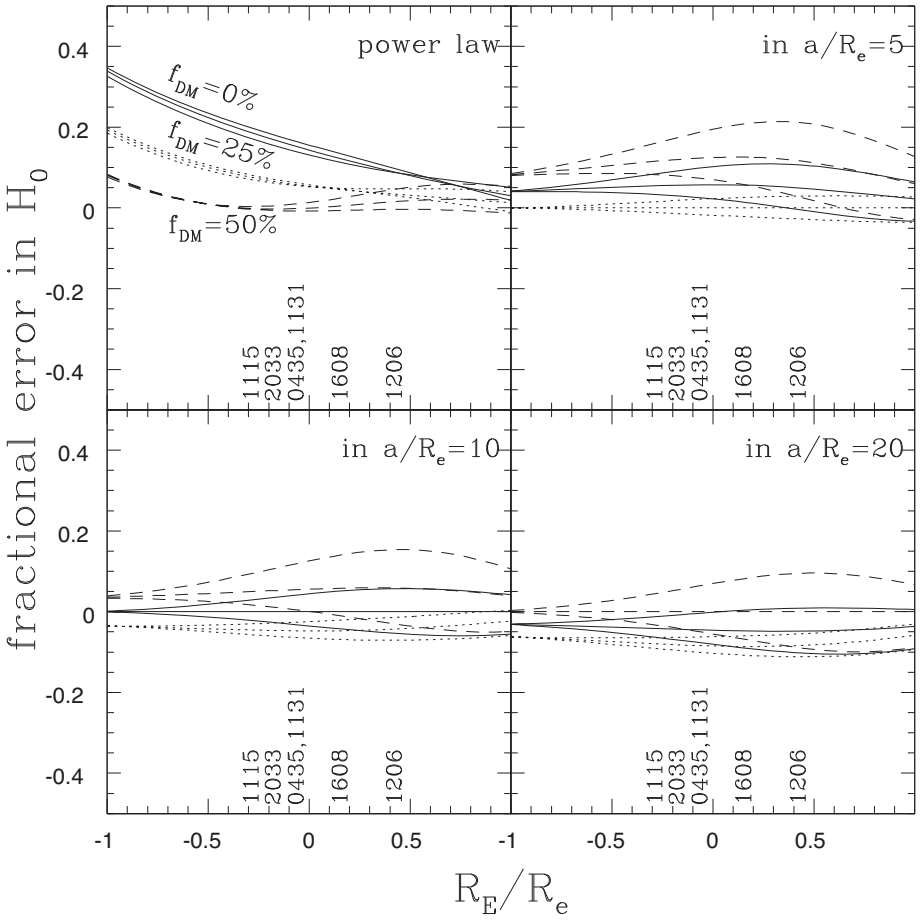

Figure 8. Fractional errors in H_0 for models with mass-to-light ratio gradients. Results are shown for fractional changes per R_e of $\mu = -0.2$ (top), 0 and 0.2 (bottom). The upper left-hand panel for the power-law models shows the cases with $f_{DM} = 0$, 25, and 50 per cent. The other three panels are for the deV+NFW models where the input model has $f_{DM} = 25$ per cent and $a/R_E = 5$ (top right), 10 (lower left), or 20 (lower right) and the lens model has $a/R_E = 5$ (dashed), 10 (solid), or 20 (dotted). Generally the $\mu = 0.2$ case is at the top and the $\mu = -0.2$ case is at the bottom.

ACKNOWLEDGEMENTS

The author thanks the H0LiCOW Collaboration for answering many questions, and C. Keeton for rapidly fixing a minor problem in LENSMODEL. CSK is supported by NSF grants AST-1908952 and AST-1814440.

REFERENCES

Agnello A., Sonnenfeld A., Suyu S. H., Treu T., Fassnacht C. D., Mason C., Bradač M., Auger M. W., 2016, MNRAS, 458, 3830
Auger M. W., Treu T., Bolton A. S., Gavazzi R., Koopmans L. V. E., Marshall P. J., Moustakas L. A., Burles S., 2010, ApJ, 724, 511
Birrer S. et al., 2019, MNRAS, 484, 4726
Blumenthal G. R., Faber S. M., Flores R., Primack J. R., 1986, ApJ, 301, 27
Bolton A. S. et al., 2012, ApJ, 757, 82
Bonvin V. et al., 2017, MNRAS, 465, 4914
Bonvin V. et al., 2019, A&A, 629, A97
Bullock J. S., Kolatt T. S., Sigad Y., Somerville R. S., Kravtsov A. V., Klypin A. A., Primack J. R., Dekel A., 2001, MNRAS, 321, 559
Chen G. C.-F. et al., 2019, MNRAS, 490, 1743
Courbin F. et al., 2018, A&A, 609, A71
de Vaucouleurs G., 1948, Ann. d'Astrophys., 11, 247
Dutton A. A., Macciò A. V., 2014, MNRAS, 441, 3359
Einasto J., 1965, Trudy Astrofizicheskogo Inst. Alma-Ata, 5, 87
Gavazzi R., Treu T., Rhodes J. D., Koopmans L. V. E., Bolton A. S., Burles S., Massey R. J., Moustakas L. A., 2007, ApJ, 667, 176
Gorenstein M. V., Falco E. E., Shapiro I. I., 1988, ApJ, 327, 693
Grogin N. A., Narayan R., 1996, ApJ, 464, 92
Hernquist L., 1990, ApJ, 356, 359
Keeton C. R., 2001, preprint (arXiv:astro-ph/0102340)
Keeton C. R., 2011, Astrophysics Source Code Library, record ascl:1102.003
Kochanek C. S., 2002, ApJ, 578, 25
Kochanek C. S., 2006, in Meylan G., Jetzer P., North P., eds, Saas-Fee Advanced Course 33, Gravitational Lensing: Strong, Weak and Micro. Springer-Verlag, Berlin, p. 91
Koopmans L. V. E. et al., 2009, ApJ, 703, L51
Kormendy J., Djorgovski S., 1989, ARA&A, 27, 235
Kundić T. et al., 1997, ApJ, 482, 75
Liao K. et al., 2015, ApJ, 800, 11
Merritt D., Navarro J. F., Ludlow A., Jenkins A., 2005, ApJ, 624, L85
Moore B., Quinn T., Governato F., Stadel J., Lake G., 1999, MNRAS, 310, 1147
Muñoz J. A., Kochanek C. S., Keeton C. R., 2001, ApJ, 558, 657
Navarro J. F., Frenk C. S., White S. D. M., 1997, ApJ, 490, 493
Navarro J. F. et al., 2010, MNRAS, 402, 21
Planck Collaboration VI, 2018, preprint (arXiv:1807.06209)
Press W. H., Rybicki G. B., Hewitt J. N., 1992, ApJ, 385, 404
Reed D. S., Koushiappas S. M., Gao L., 2011, MNRAS, 415, 3177
Refsdal S., 1964, MNRAS, 128, 307

Romanowsky A. J., Kochanek C. S., 1999, ApJ, 516, 18
Rusin D., Kochanek C. S., 2005, ApJ, 623, 666
Rusu C. E. et al., 2019, preprint (arXiv:1905.09338)
Schild R. E., 1990, AJ, 100, 1771
Schneider P., Sluse D., 2013, A&A, 559, A37
Sonnenfeld A., 2018, MNRAS, 474, 4648
Suyu S. H., Marshall P. J., Auger M. W., Hilbert S., Blandford R. D., Koopmans L. V. E., Fassnacht C. D., Treu T., 2010, ApJ, 711, 201
Suyu S. H. et al., 2013, ApJ, 766, 70
Tonry J. L., 1998, AJ, 115, 1
Treu T., Koopmans L. V. E., 2002, MNRAS, 337, L6
Unruh S., Schneider P., Sluse D., 2017, A&A, 601, A77
Walsh D., Carswell R. F., Weymann R. J., 1979, Nature, 279, 381
Wertz O., Orthen B., Schneider P., 2018, A&A, 617, A140
Wong K. C. et al., 2017, MNRAS, 465, 4895
Wong K. C. et al., 2019, MNRAS, in press (arXiv:1907.04869)
Xu D., Sluse D., Schneider P., Springel V., Vogelsberger M., Nelson D., Hernquist L., 2016, MNRAS, 456, 739

This paper has been typeset from a TEX/LATEX file prepared by the author.